Effects of charge transport on polarization of strained TiO_2: A first-principles investigation

Jian Zheng, Di Wu, and Da-Jun Shu*

National Laboratory of Solid State Microstructures and School of Physics, Nanjing University, Nanjing 210093, China

(Received 3 August 2023; revised 25 March 2024; accepted 3 June 2024; published 20 June 2024)

Ferroelectric materials have potential applications in surface catalysis and photocatalysis due to the electron-hole separation induced by the built-in field. On the other hand, both the adsorption-induced charge transfer and the photogenerated free carriers influence the stability of the ferroelectric polarization. Therefore an in-depth understanding of the interaction between the charge transfer and the polarization is of the essence. In this paper, we take rutile TiO_2 under applied strain as an example to study the effects of charge transfer and charge redistribution on polarization since it is known as a high-performance photocatalytic material as well as an incipient ferroelectric material. We consider charge transfer or charge redistribution induced by surface adsorption and photoexcitation and as a function of on-site Coulomb interaction. We find that the polarization generally decreases if charge transfer occurs in the ferroelectric materials, independent of the origin of the charge transfer or charge redistribution. The pseudo-Jahn-Teller theory is successfully adopted to explain the interaction between the charge transfer and macroscopic polarization. These findings give a clear physical picture of the effect of charge transfer and charge redistribution on the stability of polarization, which could contribute to the understanding of the ferroelectric catalytic and photocatalytic materials.

DOI: 10.1103/PhysRevB.109.214108

I. INTRODUCTION

Ferroelectric materials have potential applications in surface catalysis and photocatalysis since their surfaces selectively enhance the oxidation or reduction reaction, depending on whether the bound charges on the surfaces are positive or negative, respectively [1]. In addition, macroscopic polarization of ferroelectric material is also favorable in the photocatalytic process because it can effectively separate the photogenerated charges [2–6]. Meanwhile, the charge transfer during a surface catalytic reaction might play an important role in the stability of the macroscopic polarization. Generally, the itinerant charges may screen the long-range Coulomb interaction, thus decreasing the polarization [7,8]. On the other hand, recent works confirmed the existence of ferroelectric metal and revealed that the metallic and ferroelectric states could coexist [9–11]. This calls for more studies on the interaction between the free carriers and the polarization.

Rutile TiO_2 is an incipient ferroelectric material. Under tensile strain along the [001] direction, the frequency of the A_{2u} mode decreases below zero, resulting in the transition from a paraelectric phase to a ferroelectric phase [12–15]. Meanwhile, rutile TiO_2 is also the most intensively investigated binary transition metal oxide due to its wide range of applications in the fields of energy, environment, and health [16–18]. The photoinduced free carriers and the charge transfer between adsorbate molecules and the surface are essential in most applications of TiO_2 [19]. In addition, the d-band electrons in TiO_2 are strongly correlated with each other. The correlation energy can be partly taken into account in the density function theory using the Hubbard U correction method, which, however, also changes the charge distribution between Ti and O atoms in addition to increasing the band gap [20–22]. Hence, TiO_2 can be taken as an ideal material for researching the polarization response to the charge transfer or charge redistribution caused by surface adsorption and photoexcitation and as a function of on-site Coulomb interaction correction.

In this paper, with the help of first-principles calculations, we show the adsorbates that exchange charges with the TiO_2(110) surface can substantially weaken the surface polarization and have weaker adsorption strength. As for the photogenerated charges in bulk TiO_2, although both electrons and holes can decrease polarization, polar distortion has more tolerance for hole doping than electron doping. Moreover, we illustrate that the charge redistribution as a function of the on-site Coulomb interaction also decreases the polarization in both TiO_2 and $BaTiO_3$. The pseudo-Jahn-Teller theory based on electron-lattice coupling is adopted to successfully explain the general effect of the charge transfer or redistribution on the polarization in rutile TiO_2. This work will help theoretical and experimental researchers to understand the charge transfer and redistribution effect on ferroelectricity in rutile TiO_2 and to avoid polarization reduction during the photocatalytic process by designing novel materials or surface modification [9,23,24].

II. METHODS

Our calculations are based on density function theory (DFT) implemented in the Vienna *ab initio* Simulation Package (VASP) [25]. The projector augmented-wave method [26–29] and the Perdew-Burke-Ernzerhof (PBE) exchange

*Contact author: djshu@nju.edu.cn

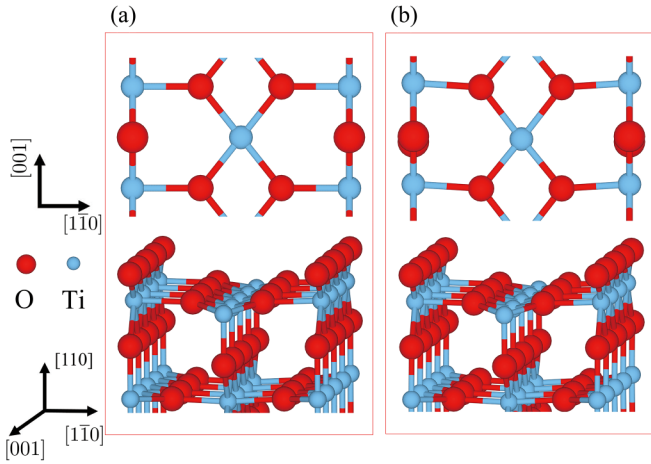

FIG. 1. Surface configurations of (a) nonpolarized and (b) polarized $TiO_2(110)$ under 4% tensile strain along the [001] direction. In the top views, only the first trilayer of a single surface unit cell is shown for clarity.

and correlation functional are used to determine the total energy [28]. The elastic constants obtained using the generalized gradient approximation PBE potential are close to the experimental results [30]. In addition, the PBE potential also effectively reproduces the polarization and charge transfer properties on TiO_2 [14,31]. The plane-wave cutoff energy is set to 600 eV to extend the Kohn-Sham wave functions. The valence configurations for Ti, O, C, N, Cl, and H are $3p^6 3d^2 4s^2$, $2s^2 2p^4$, $2s^2 2p^2$, $2s^2 2p^3$, $3s^2 3p^5$, and $1s^1$, respectively [32]. The criterion for the electron self-consistent calculation is set to 10^{-5} eV. All those atoms are relaxed without constraints until the atomic forces are converged to 0.01 eV/Å. These settings are chosen to guarantee the convergence of total energy up to 0.02 meV per atom. The Hubbard U correction is considered only in Sec. III D, where we study the influence of on-site Coulomb interaction on the polarization, and the method proposed by Dudarev is used, in which only the $U_{\text{eff}} = U - J$ term is of concern [33]. In addition, the charge transfer is obtained with the Bader charge analysis method [34].

The unit cell of rutile TiO_2 is modeled with a $6 \times 6 \times 9$ Monkhorst-Pack K point grid. The optimized lattice constants are $a = b = 4.66$ Å and $c = 2.97$ Å, in agreement with previous experimental and computational works [14,35]. They are adjusted according to the specific value of the strain along the [001] direction, followed by a full relaxation, and nonpolarized or polarized bulk structures are obtained depending on whether the symmetry is preserved or not during the relaxation [14]. Then the nonpolarized and polarized $TiO_2(110)$ surfaces are constructed based on the corresponding bulk phase, as shown in Fig. 1 for typical surface configurations under 4% tensile strain along the [001] direction. The setups for the surface relaxation and the optimized lattice parameters and direct atomic coordinates are listed in Tables S1 and S2 of the Supplemental Material [36], respectively. Each $TiO_2(110)$ surface is modeled as a (4×1) supercell consisting of a slab of five O-Ti-O trilayers and a vacuum thickness of 15 Å, with the x and y axes along the [001] and [1$\bar{1}$0] directions, respectively. In the slab system, the criterion for the electron self-consistent calculation is set to 10^{-4} eV in order to speed up the convergence. The corresponding Brillouin zone is modeled with a $3 \times 5 \times 1$ Monkhorst-Pack grid.

To monitor the convergence of the settings, the adsorption energy on the nonstrained surface is calculated; it is defined as $E_{\text{ad}}(0) = E_{\text{t}}(0) - E_{\text{s}}(0) - E_{\text{m}}$, where E_{t} and E_{s} correspond to the total energy of the structure after and before surface adsorption and E_{m} is the total energy of an isolated adsorbate molecule. If more inner electrons are considered to be valence electrons, for example, $3s^2 3p^6 3d^2 4s^2$ for Ti, we find the variation of the adsorption is smaller than 0.015 eV. Similarly, a slab thickness of six trilayers results in the variation of adsorption energy of 0.05 eV compared with the thickness of five trilayers. Since we are concerned with the adsorption energy relative to that on the nonstrained surface, the influence of the Ti s electron or a thicker slab is expected to be even smaller. In addition, the change in charge transfer is smaller than 0.006 e if Ti s electrons are considered or the slab thickness increases. Therefore, the current settings are reasonable for the aim of a study considering the balance between efficiency and accuracy. It is worth mentioning that although the surface energy of the $TiO_2(110)$ surface oscillates with the slab thickness up to eight trilayers [37,38], a slab with five trilayers turns out to be thick enough with regard to the convergence demand of the current work.

The change in adsorption energy of an adsorbate on the strained substrate relative to the nonstrained surface is defined as follows:

$$\delta E_{\text{ad}}(\varepsilon) = [E_{\text{t}}(\varepsilon) - E_{\text{s}}(\varepsilon)] - [E_{\text{t}}(0) - E_{\text{s}}(0)], \qquad (1)$$

where $E_{\text{t}}(\varepsilon)$ and $E_{\text{s}}(\varepsilon)$ are the total energies with and without adsorbates on the $TiO_2(110)$ surface under uniaxial strain ϵ along the [001] direction, respectively.

III. RESULTS

A. Tensile strain induced polarization

First of all, we demonstrate and quantitatively describe the polarization induced by the external tensile strain. It is well known that the frequency of the A_{2u} optical mode in rutile TiO_2 decreases below zero under [001] uniaxial tensile strain, which implies that a transition occurs from a paraelectric phase to a ferroelectric phase [14,39,40]. The displacements along the [001] direction of Ti and O atoms are labeled u_{Ti} and u_{O}, respectively. The displacement of Ti relative to O, $u_{\text{Ti}} - u_{\text{O}}$, denoted as u, is correlated with the strain-induced polarization. The strain-induced polarization in TiO_2 is similar to the situation in $SrTiO_3$ and $CaTiO_3$ [13,41].

In order to show the stability of strain-induced polarization in rutile TiO_2, we plot in Fig. 2(b) the energy variation as a function of u by gradually shifting Ti atoms along the [001] direction and fixing the O atoms at their high-symmetry positions. Apparently, the off-center relaxation is energetically favorable. The most favorable displacement of Ti relative to O, denoted as δu, increases with increasing tensile strain, as shown in the inset of Fig. 2(b). Furthermore, we plot in the inset of Fig. 2(b) the energy of the low-symmetry ferroelectric phase relative to the high-symmetry phase δF as a function of the tensile strain along the [001] direction. Obviously, the

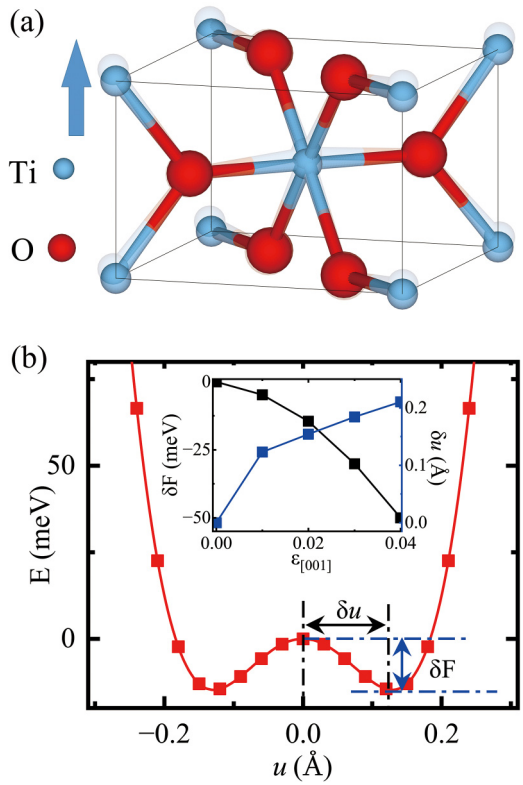

FIG. 2. (a) Ball and stick model of rutile TiO_2. The transparent and opaque balls represent the atom in the low-symmetry ferroelectric and high-symmetry paraelectric phases, respectively. The blue arrow denotes the displacements of Ti atoms relative to the O atoms. (b) The total energy variation as a function of the Ti gradual shift along the [001] direction when 2% tensile strain is applied along the [001] direction. The black and blue curves in the inset of (b) correspond to the energy and the Ti position of the ferroelectric phase relative to the paraelectric phase, δF and δu, as a function of the uniaxial strain, respectively.

ferroelectric phase becomes more stable when larger tensile strain along the [001] direction is applied.

This result confirms that rutile TiO_2 is an incipient ferroelectric material, consistent with previous results [14]. Moreover, it suggests that the external tensile strain is a useful way to control the stability of polarization. Therefore, we study the interaction between the ferroelectric polarization and the charge transfer by applying different tensile strains along the [001] direction in rutile TiO_2. In this work we consider three kinds of charge transfer with different origins, namely, the adsorption-induced charge transfer on the TiO_2(110) surfaces (Sec. III B), the photogenerated carriers in bulk TiO_2 (Sec. III C), and the on-site interaction induced charge distribution in bulk TiO_2 (Sec. III D).

B. Adsorption-induced charge transfer

To explore the interaction between the charge transfer induced by surface adsorption and the polarization, we consider the most stable and most studied rutile TiO_2(110) surface under strain ranging from 0.01 to 0.04 along the [001] direction [14,42]. First, we study the change in polarization induced by surface adsorption. Then we unravel the effect of polarization on the surface adsorption by comparing the adsorption energy on the polarized and nonpolarized TiO_2(110) surfaces.

TABLE I. Summary of the adsorption properties of the four adsorbates on the TiO_2(110) surface. A positive value means the electrons are transferred from adsorbates to the substrate. Both the charge transfer and the adsorption energy are calculated for the nonstrained, nonpolarized substrate.

	Adsorbate molecule			
	CO	HCl	Cl	N_2
Polarity molecule	Yes	Yes	No	No
Charge transfer (e)	0.03	0.12	−0.42	0.01
δE_{ad} (eV)	−0.31	−1.27	−1.37	−0.14

Four adsorbates are considered, namely, HCl, Cl, CO, and N_2, each with a coverage of 1/4. Among the four kinds of adsorbates, HCl and CO are polar molecules, while N_2 and Cl are nonpolar. The most stable adsorption configurations on the nonstrained surface are shown in Fig. 3, consistent with the results in previous works [43–49]. For HCl, the dissociative configuration is favorable, with the hydrogen and chlorine atoms bonding with the bridge oxygen and five-coordinated titanium (Ti_{5c}), respectively. The Cl_2 molecule also dissociates, with the two Cl atoms sitting on two separate surface Ti_{5c} sites [44]. Here, the adsorption of only one Cl atom is considered for simplicity. For CO, the C atom binds with Ti_{5c}, and the C-O bond is perpendicular to the surface. N_2 has an adsorption configuration similar to that of CO, with one of the nitrogen atoms binding with the surface Ti_{5c}. The adsorption energies $E_{ad}(0)$ on the nonstrained substrate and the charge transfer between the adsorbates and the substrate are listed in Table I. It is clear that HCl and Cl dope electrons and holes to the substrate, respectively. However, CO and N_2 have little charge exchange with the substrate. Meanwhile, HCl and Cl bind more strongly than CO and N_2 with the substrate. This suggests that the binding strength is highly correlated with the charge transfer.

The change in the density of states (DOS) of the substrate also provides evidence for the charge exchange between the substrate and adsorbates. As shown in Fig. S1 in the Supplemental Material, the DOS of the substrate changes little after CO and N_2 are adsorbed on the surface. As for the adsorption of HCl and Cl, the DOS of the O p orbit decreases around an energy of −1 eV (relative to the Fermi level). Furthermore, the orbit occupation based on the DOS of the substrate shows that the Ti d orbit occupation increases, while the O p orbit occupation decreases after the adsorption of HCl and Cl. The changes in the DOS of substrate are consistent with the charge transfer results listed in Table I. The doped charge is localized at the surface Ti_{5c} and bridging O atoms that bind with the adsorbate, as shown in Fig. S2 in the Supplemental Material.

The adsorption configurations on the strained surface are constructed based on the corresponding nonstrained ones by adjusting the lattice parameter according to the specific strain, followed by a full relaxation. It is worth mentioning that the

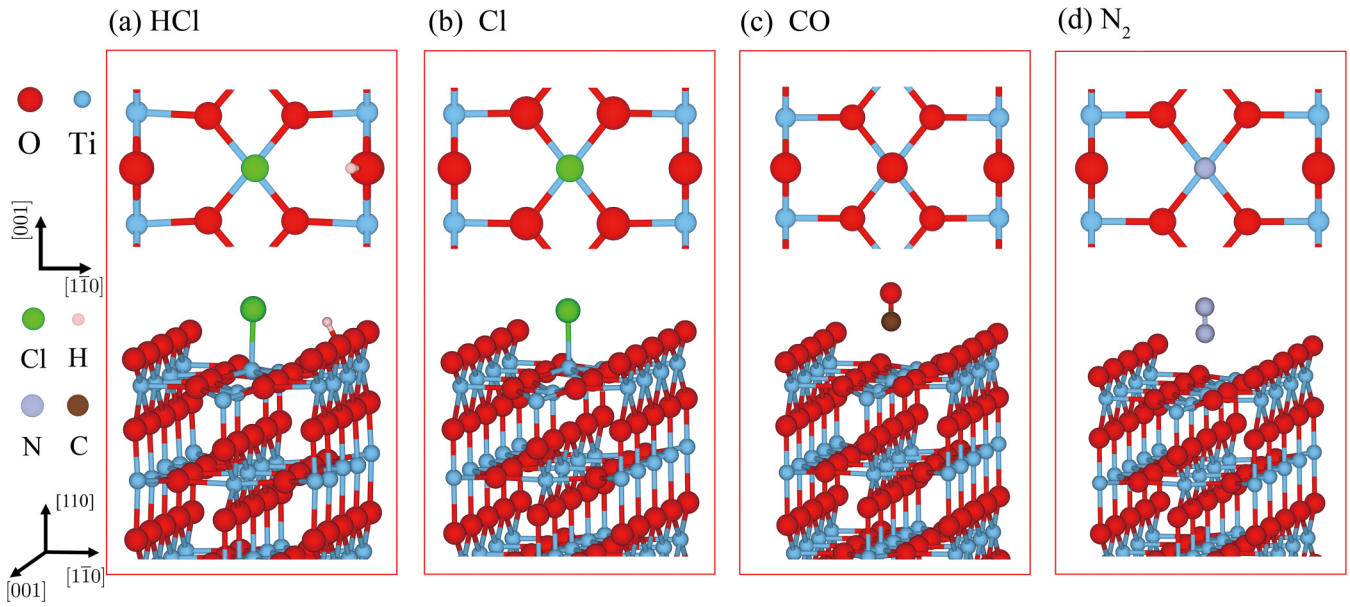

FIG. 3. Atomic configurations of different adsorbates, (a) HCl, (b) Cl, (c) CO, and (d) N_2, on the nonstrained TiO_2(110) surface. The top panels show top views of the first trilayer of the unit cell containing the adsorbates.

nonpolarized state of the strained surface is metastable against the polarized one since none of the considered adsorption configurations break the mirror-plane symmetry of the [001] direction.

The adsorption-induced polarization variation is evaluated using the average change in the atomic displacement after the surface adsorption. We stress that although the change in polar off-centering displacement with surface adsorption occurs for all the Ti and O atoms, the response of the topmost surface atoms within a single surface unit cell around the adsorption site contributes about 65% (HCl), 57% (Cl), 43% (CO), or 46% (N_2) to the overall off-centering displacement. Specifically, when Cl, CO, and N_2 are adsorbed on the polarized surfaces, only the displacement of the surface Ti_{5c} atom that binds with the adsorbate contributes dominantly to the change in polar off-centering. As for the adsorption of HCl on the polarized surface, the displacement of the Ti_{6c} atoms close to H atom also contributes evidently to the change of polar off-centering. The average distortion upon the adsorption is calculated by $\overline{\Delta u} = u' - u = \overline{u'_{\mathrm{Ti}} - u_{\mathrm{Ti}}} - \overline{u'_{\mathrm{O}} - u_{\mathrm{O}}}$. We note that the displacement of Ti is almost twice that of O. Therefore, the distortion upon the adsorption mainly comes from $\overline{u'_{\mathrm{Ti}} - u_{\mathrm{Ti}}}$. As the polarization is along the [001] direction, a negative $\overline{\Delta u}$ means the polar distortion is weakened by the surface adsorption.

As shown in Fig. 4, the polar distortion is nearly unchanged when CO or N_2 is adsorbed on the surface. Instead, it decreases significantly when HCl or Cl attaches. According to the results listed in Table I, this indicates that the adsorption-induced charge transfer drastically weakens the substrate polarization. Furthermore, it is worth mentioning that the magnitude of the polarization reduction induced by HCl is greater than the one induced by Cl. This suggests that the doped electrons and holes have a different impact on the substrate polarization, which will be discussed later in Sec. IV.

The polarization of the substrate, in turn, also has an effect on the surface adsorption. In order to describe this effect quantitatively, we plot in Fig. 5 the variation of the adsorption energy with the external applied strain, where $\delta E_{\mathrm{ad}}^{\mathrm{pl}}$ and $\delta E_{\mathrm{ad}}^{\mathrm{np}}$ are the adsorption energies on the polarized and nonpolarized surfaces, respectively. As shown in Fig. 5, the adsorption energies of different adsorbates on the nonpolarized surfaces decrease with the tensile strain with different slopes. This originates from the adsorption-induced decrease in the surface stress. We find that the changes in the surface stress are −1.37, −0.22, −0.20, and −0.13 eV/(1 × 1) with the adsorption of HCl, Cl, CO, and N_2, respectively. Therefore, the adsorption energy of HCl is expected to decrease with strain most dramatically, as shown in Fig. 5(a). For the polarized surface, the adsorption-induced changes in the surface stress are −1.25, −0.37, −0.40, and −0.21 eV/(1 × 1) for the adsorption of HCl, Cl, CO, and N_2, respectively. Clearly, the difference in surface stress caused by adsorption between polarized and nonpolarized surfaces is not large enough to be responsible for the large difference in the slope between the polarized

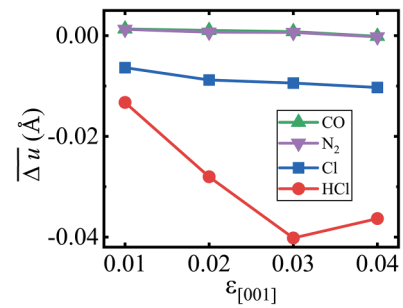

FIG. 4. The variation of $\overline{\Delta u}$ as a function of tensile strain along the [001] direction. The different colored curves represent different adsorbates.

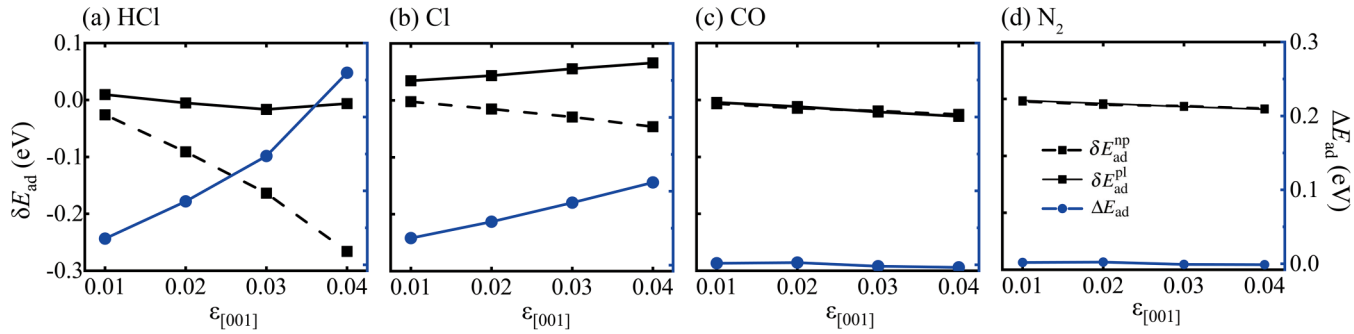

FIG. 5. The strain-induced change in adsorption energy δE_{ad} of different adsorbates: (a) HCl, (b) Cl, (c) CO, and (d) N_2; the solid and dashed black curves correspond to the results on the polarized surface δE_{ad}^{pl} and nonpolarized surface δE_{ad}^{np}, respectively. The blue curve corresponds to ΔE_{ad} ($\Delta E_{ad} = \delta E_{ad}^{pl} - \delta E_{ad}^{np}$).

and nonpolarized surfaces. This indicates that in addition to the surface stress, the polarization of the substrate also has an effect on the surface adsorption.

In order to demonstrate the effect of polarization on the surface adsorption, the difference $\Delta E_{ad} = \delta E_{ad}^{pl} - \delta E_{ad}^{np}$ is also plotted in Fig. 5. For CO and N_2, the adsorption energies are almost the same on the polarized and nonpolarized substrates and change little with the strain. Obviously, their adsorption strength is not affected by the polarization of the substrate, although CO is polar, while N_2 is nonpolar. This suggests that the adsorption strength is hardly correlated with the dipole-dipole interaction between the adsorbate and the substrate [50]. In contrast, $\Delta E_{ad} > 0$ for HCl and Cl, which means that they bind less strongly with the polarized surface.

Clearly, there is a correlation between ΔE_{ad} and the adsorption-induced charge transfer. Whether ΔE_{ad} is nonzero or zero depends on whether adsorption-induced charge transfer occurs or not. This trend coincides with the adsorption-induced polar distortion shown in Fig. 4. It indicates that the adsorbates contribute free carriers to the polarized substrate, which increases the total energy of the substrate and thus results in weaker adsorption strength. The magnitude of this effect furthermore depends on whether the contributed carrier is an electron or hole. As can be seen in Fig. 5, although HCl contributes fewer carriers than Cl, the reduction in ΔE_{ad} is more dramatic with the strain. This indicates that the polarization is affected more dramatically by the doped electrons than holes. The reason will be discussed later.

The above discussion shows that the adsorption-induced charge transfer indeed decreases the substrate polarization on the TiO_2(110) surface. In addition, the polarization has more tolerance for the adsorption with hole transfer to the substrate than that with electron transfer. These conclusions are consistent with our previous simulation [50]. Moreover, an experimental work on a $BaTiO_3$(001) thin film reported that the out-of-plane surface polarization is weakened when charge exchanges between the adsorbate and substrate [51], which is consistent with the conclusion of this work.

C. Photogenerated charges

In photocatalytic materials, besides the adsorption-induced charges, photogenerated charges are also inevitable and will have a significant impact on the stability of polarization. The interaction between photogenerated carriers and the surface polarization has been demonstrated. Using x-ray photoelectron spectroscopy, Wang *et al.* found that photogenerated free carriers effectively screen the surface polarization charges in $BaTiO_3$ [52]. Shao *et al.* noticed a significant and gradual potential drop between positive and negative $BaTiO_3$(001) surfaces after the sample was illuminated [53]. Those experimental works clearly suggest that the itinerant charges decrease the polarization.

Here, we compare the influence of additional electrons and holes on the polarization with first-principles calculations. We stress that the exciton radius in rutile TiO_2 is about 40 Å, which is much larger than the lattice constant [54]. Therefore, it is reasonable to separately study the electrons and holes in order to mimic the photoexcitation. Extra electrons or holes from 0 to 1 e per unit cell are doped in the TiO_2 bulk phase to mimic the photogenerated charges by controlling the number of total electrons [55]. Different tensile strains ranging from 0.005 to 0.045 are applied along the [001] direction to stabilize and control the polarization. The value of δu is taken as a descriptor of the polarization. Obviously, a larger δu means stronger polarization. The variation of δu as a function of the strain and the doped charges is plotted in Fig. 6. We can find that although the tensile strain along the [001] direction

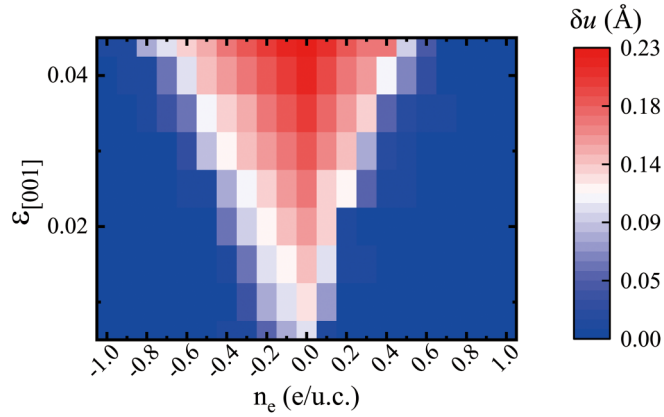

FIG. 6. The heat map of δu as a function of the doping concentration and tensile strain along the [001] direction. The negative and positive values of n_e stand for the hole doping and electron doping, respectively.

finally stabilizes the polarization, the onset strain increases with increasing concentration of the doped charges. Under the same tensile strain, the higher the doped electron or hole concentration is, the weaker the polarization is. These phenomena suggest that the doped charges tend to destabilize the polarization, whether the doped charge is an electron or hole. However, the doped electrons and holes have asymmetrical influence on the destabilizing polarization of the rutile bulk TiO_2, with greater tolerance for holes compared with electrons. This is consistent with the case of surface adsorption shown in Sec. III B, where we found that the polarization is affected more dramatically by the adsorption-induced electrons than holes. Previous DFT studies also confirmed that a doped electron destabilizes polarization, while a doped hole has less influence on the polarization in $BaTiO_3$ [56,57]. The charge transfer induced by adsorption and the charge doping effect have a quite similar influence on the polarization. The underlying mechanism will be discussed in Sec. IV.

D. On-site Coulomb interaction

In rutile TiO_2, experimental studies showed the electronic band gap is about 3.0 eV, while many theoretical studies with the PBE functional resulted in a band gap of about 1.9 eV. This underestimation of the band gap energy originates from the fact that the DFT cannot precisely describe Ti strongly correlated $3d$ electrons [58], which is known as a generic problem of DFT. On-site Coulomb interaction correction is a useful way to remedy this underestimation by removing the self-interaction error. However, the Hubbard U is an empirical parameter, and it is difficult to determine Hubbard's U with experimental methods [59]. Theoretically, like for rutile TiO_2, the range of Hubbard's U is between 2 and 6 eV, depending on the properties that researchers are interested in [60]. Here, we set U to be different values in order to find the effect of the change in Hubbard's U on the polarization. The effect of Hubbard's U on the polarization is considered from the aspect of charge redistribution among Ti and O since the on-site Coulomb interaction reduces the mixing between Ti $3d$ and O $2p$ [61]. From this perspective, we vary the on-site Coulomb interaction to trigger the third kind of charge transfer in this paper.

We carry out PBE+U calculations for bulk polarized rutile TiO_2 structures with U_{eff} changing from 1 to 6, where U_{eff} signifies the strength of on-site Coulomb interaction. As shown in Fig. 7, the band gap increases with U_{eff}. Meanwhile, the electron occupation number of the $3d$ orbit decreases with increasing U_{eff}. This means that the on-site Coulomb interaction causes electron transfer from the Ti $3d$ to O $2p$ orbit [61,62]. The charge redistribution along with increasing on-site Coulomb interaction is more significant for larger tensile strain.

The polarization of bulk rutile TiO_2 as a function of U_{eff} under different [001] tensile strains is calculated using the Berry phase method and plotted in Fig. 8 [63–65]. For comparison, the polarization variation with the on-site Coulomb interaction in $BaTiO_3$, a conventional ferroelectric material, is also calculated and shown in Fig. 8 [66]. It is obvious that the polarization decreases with increasing U_{eff} for both strained TiO_2 and $BaTiO_3$. This means that the polarization

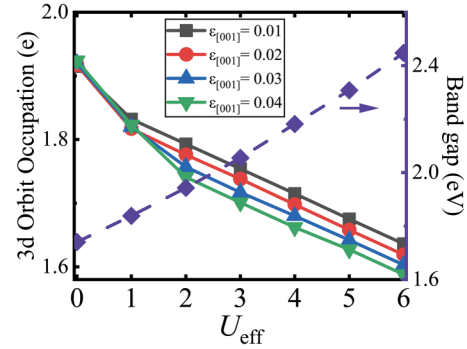

FIG. 7. The variation of $3d$ orbit occupation as a function of U_{eff}. The solid lines show the rutile TiO_2 bulk structures under different strains along the [001] direction. The purple dashed curve is the change in band gap as a function of U_{eff} in the nonstrained structure, as denoted by the purple arrow.

tends to be destabilized when the on-site Coulomb interaction in Ti $3d$ electrons is included. Previous works also showed the same trend in some multiferroics such as $HoMn_2O_5$ and $TbMn_2O_5$ [67,68]. We propose that the polarization reduction as a function of the on-site Coulomb interaction is mediated by the charge transfer between Ti and O. In the next section we will further verify this proposal.

IV. UNDERSTANDING THE MECHANISM: PSEUDO-JAHN-TELLER EFFECT WITH CHARGE TRANSFER

The pseudo-Jahn-Teller (PJT) effect, which was first proposed in 1957 [69], is considered the source of structural instability of high-symmetry configurations of polyatomic systems in nondegenerate states [70]. In the PJT effect, the lattice-electron coupling is important for the distortions of high-symmetry configurations. The coupling results in the variation of the force constant, which is the second derivative of the adiabatic potential energy surface. The force constant may become negative in some directions, which means the

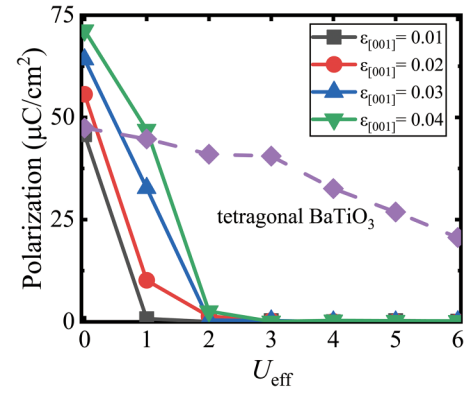

FIG. 8. The variation of the polarization as a function of U_{eff}. The solid curves show the rutile TiO_2 bulk structures under different strains along the [001] direction; the purple dashed curve shows the tetragonal $BaTiO_3$ structure. The results of both strained rutile TiO_2 and tetragonal $BaTiO_3$ suggest that the on-site Coulomb interaction decreases the polarization.

distortion is favorable in those directions, resulting in a transition from the paraelectric phase to the ferroelectric phase.

For the purpose of illustrating the response of the polarization to the charge transfer or charge redistribution, we adopt the PJT theory to explain polar distortion [70,71]. In the single-electron approximation, the ground state and excited state of the high-symmetry configuration are the valence band (VB) and the conduction band (CB), respectively. Obviously, the "d^0" rule means the VB mainly comprises the O $2p$ orbit, while the CB mainly comprises the Ti $3d$ orbit. Here, we define the two-level off-diagonal vibronic coupling constant as $f = \langle 2p|(\frac{\partial H}{\partial Q})_0|3d\rangle$. The primary force constants for the VB and CB are defined as $K_{01} = \langle 2p|(\frac{\partial^2 H}{\partial Q^2})_0|2p\rangle$ and $K_{02} = \langle 3d|(\frac{\partial^2 H}{\partial Q^2})_0|3d\rangle$, respectively. When the VB and CB interact under the linear vibronic coupling, we get the following equation under linear vibronic coupling [70,71]:

$$\begin{vmatrix} \frac{1}{2}K_{01}Q^2 - \Delta - \mathcal{E} & fQ \\ fQ & \frac{1}{2}K_{02}Q^2 + \Delta - \mathcal{E} \end{vmatrix} = 0, \tag{2}$$

where $\mathcal{E}$ is the band eigenenergy relative to the middle of the energy gap, Δ is half of the energy gap between the VB and CB, and Q is the displacement of Ti atoms. We can expand the energy $\mathcal{E}$ to the second term of Q^2 as follows:

$$\mathcal{E}_1(Q) = -\Delta + \frac{1}{2}\left(K_{01} - \frac{f^2}{\Delta}\right)Q^2 + \frac{1}{8}\frac{f^2[f^2 - (K_1 - K_2)\Delta]}{\Delta^3}Q^4 + \cdots, \tag{3}$$

$$\mathcal{E}_2(Q) = \Delta + \frac{1}{2}\left(K_{02} + \frac{f^2}{\Delta}\right)Q^2 - \frac{1}{8}\frac{f^2[f^2 - (K_1 - K_2)\Delta]}{\Delta^3}Q^4 + \cdots. \tag{4}$$

Therefore, the curvatures of the VB and CB as a function of displacement are

$$K_1 = K_{01} - \frac{f^2}{\Delta}, \quad K_2 = K_{02} + \frac{f^2}{\Delta}. \tag{5}$$

It was proved that in any polyatomic system in the high-symmetry configuration, K_{01} and K_{02} are positive [70]. This leads to positive K_2. Clearly, a negative K_1 is necessary for polar distortion. According to Eq. (5), the VB treated as ground states is softened, while the CB treated as excited states is hardened. We define q_1 and q_2 as the electron populations of the VB and CB, respectively. Then the total force constant K for the electron-lattice coupling is $K = q_1K_1 + q_2K_2$ [72]. According to the PJT theory, a negative force constant K is vital for the polar distortion. Moreover, the polar distortion is weakened when K increases.

Now we consider the effect of charge doping on the relative stability of polarization. The different effects of doped electrons and holes on the polarization can be attributed to the different force constants of Ti $3d$ (CB) and O $2p$ (VB). As the extra electrons are doped in the CB, q_2 increases and further results in larger K, which means weaker polarization. While the extra holes are doped, q_1 decreases, so K increases since K_1 is negative, which also makes the polarization weaker. As the concentration of doped electrons or holes increases to a certain concentration, K finally becomes positive or negligible, and the polarization is no longer stable. The trend which PJT theory predicts is consistent with the results obtained in Secs. III B and III C. In addition, the absolute value of K_1 is smaller than K_2 due to positive K_{01} and K_{02}. This means that when compared with hole doping of the same magnitude, the additional electron occupation in the CB causes a larger force constant. This coincides with the result that the electron doping and hole doping have an asymmetric influence on polarization, with more tolerance for the hole doping compared with the electron doping. In this case, we confirm that the mechanism of the charge transfer induced by the adsorption and the charge doping influence on polarization both originate from the PJT effect.

This can also explain the experimental outcome that the photogenerated electron-hole pairs decrease the bulk polarization [52,53]. The reduced q_1 and the increased q_2 caused by photogenerated electron-hole pairs both result in a larger force constant. As a consequence, the force constant K increases even more with the number of photogenerated electron-hole pairs, further leading to destabilized polarization.

We can also explain the effect of on-site Coulomb interaction on the polarization in Sec. III D with PJT theory. In contrast to the adsorption-induced or photoinduced charge transfer, the reduction of Ti $3d$ orbit occupation indicates that the charge redistribution occurs between Ti and O atoms along with increasing on-site Coulomb interaction [62]. According to Eq. (5), as the on-site Coulomb interaction enlarges the band gap, it causes weaker coupling between the VB and CB and thus leads to a larger force constant. This trend is consistent with the results shown in Fig. 8.

In previous works, the PJT mechanism was used to explain the free carrier effect on the polarization [57]. Previous experimental works found that both photogenerated carriers and adsorption-induced charges can screen the surface polarization charge in tetragonal $BaTiO_3$ [52,53]. A theoretical study found that the reduction in the polar distortion in doped $BaTiO_3$ can be explained by using the PJT effect [57].

It is worth mentioning that in the above discussion, we consider only the two-level problem. In real situations, the vibronic coupling between the CB and VB may involve more than two levels, with different coupling constants for different levels. If the lower CB level couples more weakly than the higher CB with the VB states, the ferroelectric metal can be realized by doping electrons in the lower CB level [10,56]. Similarly, if a specific highest VB level couples more weakly than the lower VB levels with the CB states, the ferroelectric metal may be realized by hole doping.

V. CONCLUSION

In this paper, we studied the effect of charge transfer or charge redistribution originating from surface adsorption and photoexcitation and as a function of on-site Coulomb interaction on the polarization of rutile TiO_2 using first-principles calculations. We found that the doped carriers will always

reduce the polar distortion and the polarization has more tolerance for hole doping compared with electron doping. In terms of adsorption-induced charge transfer, the exchanged charges destabilize the substrate polarization and result in weaker adsorption strength. In the same way, the photogenerated charge weakens the polarization and lowers the efficiency of the photocatalyst. Similarly, increasing the on-site Coulomb interaction causes a change in the electron structure and thus decreases the polar distortion. Therefore, we confirmed that the effect of charge doping is independent of the specific origins of the charge transfer. Furthermore, we provided an intrinsic mechanism to understand this effect by simply considering the coupling between the VB and CB based on pseudo-Jahn-Teller theory.

Based on our conclusion, we proposed two methods to avoid the polarization reduction when free carriers are introduced. The first one uses some novel materials like ferroelectric metals. The reason is that the mobile carriers cannot fully screen the polarization in these materials due to the unique lattice-electron coupling [23]. The other method is to build a ferroelectric tunnel junction structure with a thick metal electrode on the surface. This structure can maintain the polarization because the metal layer can screen the adsorption-induced free carriers [24,73]. These strategies can stabilize the polarization and help researchers promote the efficiency of ferroelectric catalysis or photocatalysis.

ACKNOWLEDGMENTS

The numerical calculations were carried out at the High Performance Computing Center of Nanjing University. This work was supported by the National Natural Science Foundation of China (Grants No. 11974164, No. 12274211, and No. 52025012).

[1] M. Sakar, S. Balakumar, P. Saravanan, and S. Bharathkumar, Particulates vs fibers: Dimension featured magnetic and visible light driven photocatalytic properties of Sc modified multiferroic bismuth ferrite nanostructures, Nanoscale **8**, 1147 (2016).

[2] Z. Liang, C.-F. Yan, S. Rtimi, and J. Bandara, Piezoelectric materials for catalytic/photocatalytic removal of pollutants: Recent advances and outlook, Appl. Catal., B **241**, 256 (2019).

[3] C. Hu, S. Tu, N. Tian, T. Ma, Y. Zhang, and H. Huang, Photocatalysis enhanced by external fields, Angew. Chem., Int. Ed. **60**, 16309 (2021).

[4] L. Liu, H. Huang, Z. Chen, H. Yu, K. Wang, J. Huang, H. Yu, and Y. Zhang, Synergistic polarization engineering on bulk and surface for boosting CO_2 photoreduction, Angew. Chem., Int. Ed. **60**, 18303 (2021).

[5] Y. Liu, S. Ye, H. Xie, J. Zhu, Q. Shi, N. Ta, R. Chen, Y. Gao, H. An, W. Nie, H. Jing, F. Fan, and C. Li, Internal-field-enhanced charge separation in a single-domain ferroelectric $PbTiO_3$ photocatalyst, Adv. Mater. **32**, 1906513 (2020).

[6] F. Chen, H. Huang, L. Guo, Y. Zhang, and T. Ma, The role of polarization in photocatalysis, Angew. Chem., Int. Ed. **58**, 10061 (2019).

[7] W. Renn, Screening of impurity pseudopotentials in polar semiconductors, Z. Naturforsch., A **33**, 1261 (1978).

[8] D. Alikin, A. Abramov, A. Turygin, A. Ievlev, V. Pryakhina, D. Karpinsky, Q. Hu, L. Jin, V. Shur, A. Tselev, and A. Kholkin, Exploring charged defects in ferroelectrics by the switching spectroscopy piezoresponse force microscopy, Small Methods **6**, 2101289 (2022).

[9] Y. Shi, Y. Guo, X. Wang, A. J. Princep, D. Khalyavin, P. Manuel, Y. Michiue, A. Sato, K. Tsuda, S. Yu, M. Arai, Y. Shirako, M. Akaogi, N. Wang, K. Yamaura, and A. T. Boothroyd, A ferroelectric-like structural transition in a metal, Nat. Mater. **12**, 1024 (2013).

[10] X. He and K.-J. Jin, Persistence of polar distortion with electron doping in lone-pair driven ferroelectrics, Phys. Rev. B **94**, 224107 (2016).

[11] H. J. Xiang, Origin of polar distortion in $LiNbO_3$–type "ferroelectric" metals: Role of *a*-site instability and short-range interactions, Phys. Rev. B **90**, 094108 (2014).

[12] P. D. Mitev, K. Hermansson, B. Montanari, and K. Refson, Soft modes in strained and unstrained rutile TiO_2, Phys. Rev. B **81**, 134303 (2010).

[13] V. V. Lemanov, Phase transitions in perovskite solid solutions with incipient ferroelectrics, Ferroelectrics **302**, 169 (2004).

[14] A. Grünebohm, P. Entel, and C. Ederer, First-principles investigation of incipient ferroelectric trends of rutile TiO_2 in bulk and at the (110) surface, Phys. Rev. B **87**, 054110 (2013).

[15] C. Lee, P. Ghosez, and X. Gonze, Lattice dynamics and dielectric properties of incipient ferroelectric TiO_2 rutile, Phys. Rev. B **50**, 13379 (1994).

[16] C. Zhao, J. Wang, X. Zhao, Z. Du, R. Yang, and J. Tang, Recent advances, challenges and prospects in ternary organic solar cells, Nanoscale **13**, 2181 (2021).

[17] K. Nakata, T. Ochiai, T. Murakami, and A. Fujishima, Photoenergy conversion with TiO_2 photocatalysis: New materials and recent applications, Electrochim. Acta **84**, 103 (2012).

[18] M. M. Rashid, P. Forte Tavčer, and B. Tomšič, Influence of titanium dioxide nanoparticles on human health and the environment, Nanomaterials **11**, 2354 (2021).

[19] R. Rousseau, V.-A. Glezakou, and A. Selloni, Theoretical insights into the surface physics and chemistry of redox-active oxides, Nat. Rev. Mater. **5**, 460 (2020).

[20] A. Rubio-Ponce, A. Conde-Gallardo, and D. Olguín, First-principles study of anatase and rutile TiO_2 doped with Eu ions: A comparison of GGA and LDA + U calculations, Phys. Rev. B **78**, 035107 (2008).

[21] M. E. Arroyo-de Dompablo, A. Morales-Garcia, and M. Taravillo, DFT+U calculations of crystal lattice, electronic structure, and phase stability under pressure of TiO_2 polymorphs, J. Chem. Phys. **135**, 054503 (2011).

[22] S.-D. Mo and W. Y. Ching, Electronic and optical properties of three phases of titanium dioxide: Rutile, anatase, and brookite, Phys. Rev. B **51**, 13023 (1995).

[23] C. Ke, J. Huang, and S. Liu, Two-dimensional ferroelectric metal for electrocatalysis, Mater. Horiz. **8**, 3387 (2021).

[24] H. F. Li, W. J. Chen, and Y. Zheng, First-principle study of CO adsorption influence on the properties of ferroelectric tunnel junctions, Phys. Chem. Chem. Phys. **18**, 31115 (2016).

[25] G. Kresse and J. Hafner, *Ab initio* molecular-dynamics simulation of the liquid-metal–amorphous-semiconductor transition in germanium, Phys. Rev. B **49**, 14251 (1994).

[26] G. Kresse and D. Joubert, From ultrasoft pseudopotentials to the projector augmented-wave method, Phys. Rev. B **59**, 1758 (1999).

[27] P. E. Blöchl, Projector augmented-wave method, Phys. Rev. B **50**, 17953 (1994).

[28] J. P. Perdew, K. Burke, and M. Ernzerhof, Generalized gradient approximation made simple, Phys. Rev. Lett. **77**, 3865 (1996).

[29] J. P. Perdew, J. A. Chevary, S. H. Vosko, K. A. Jackson, M. R. Pederson, D. J. Singh, and C. Fiolhais, Atoms, molecules, solids, and surfaces: Applications of the generalized gradient approximation for exchange and correlation, Phys. Rev. B **46**, 6671 (1992).

[30] A. Grünebohm, C. Ederer, and P. Entel, Reply to "Comment on 'First-principles study of the influence of (110)-oriented strain on the ferroelectric properties of rutile TiO_2,' " Phys. Rev. B **88**, 136102 (2013).

[31] T. Pabisiak and A. Kiejna, First-principles study of Au nanostructures on rutile TiO_2(110), Phys. Rev. B **79**, 085411 (2009).

[32] Y. Wang, T. Sun, X. Liu, H. Zhang, P. Liu, H. Yang, X. Yao, and H. Zhao, Geometric structure of rutile titanium dioxide (111) surfaces, Phys. Rev. B **90**, 045304 (2014).

[33] S. L. Dudarev, G. A. Botton, S. Y. Savrasov, C. J. Humphreys, and A. P. Sutton, Electron-energy-loss spectra and the structural stability of nickel oxide: An LSDA+U study, Phys. Rev. B **57**, 1505 (1998).

[34] R. F. W. Bader, A quantum theory of molecular structure and its applications, Chem. Rev. **91**, 893 (1991).

[35] B. Montanari and N. M. Harrison, Pressure-induced instabilities in bulk TiO_2 rutile, J. Phys.: Condens. Matter **16**, 273 (2004).

[36] See Supplemental Material at http://link.aps.org/supplemental/10.1103/PhysRevB.109.214108 for the calculation setups, the density of states and the differential charge density.

[37] F. Labat, P. Baranek, and C. Adamo, Structural and electronic properties of selected rutile and anatase TiO_2 surfaces: An *ab initio* investigation, J. Chem. Theory Comput. **4**, 341 (2008).

[38] H. Perron, C. Domain, J. Roques, R. Drot, E. Simoni, and H. Catalette, Optimisation of accurate rutile TiO_2 (110), (100), (101) and (001) surface models from periodic DFT calculations, Theor. Chem. Acc. **117**, 565 (2007).

[39] K. Refson, B. Montanari, P. D. Mitev, K. Hermansson, and N. M. Harrison, Comment on "First-principles study of the influence of (110)-oriented strain on the ferroelectric properties of rutile TiO_2," Phys. Rev. B **88**, 136101 (2013).

[40] A. Grünebohm, C. Ederer, and P. Entel, First-principles study of the influence of (110)-oriented strain on the ferroelectric properties of rutile TiO_2, Phys. Rev. B **84**, 132105 (2011).

[41] K. A. Müller and H. Burkard, $SrTiO_3$: An intrinsic quantum paraelectric below 4 K, Phys. Rev. B **19**, 3593 (1979).

[42] L. Jia, D.-J. Shu, and M. Wang, Tuning the area percentage of reactive surface of TiO_2 by strain engineering, Phys. Rev. Lett. **109**, 156104 (2012).

[43] H. H. Kristoffersen, J.-E. Shea, and H. Metiu, Catechol and HCl adsorption on TiO_2(110) in vacuum and at the water–TiO_2 interface, J. Phys. Chem. Lett. **6**, 2277 (2015).

[44] D. Vogtenhuber, R. Podloucky, J. Redinger, E. L. D. Hebenstreit, W. Hebenstreit, and U. Diebold, *Ab initio* and experimental studies of chlorine adsorption on the rutile TiO_2(110) surface, Phys. Rev. B **65**, 125411 (2002).

[45] A. Fahmi and C. Minot, A theoretical study of CO adsorption on TiO_2, J. Organomet. Chem. **478**, 67 (1994).

[46] D. C. Sorescu and J. J. T. Yates, First principles calculations of the adsorption properties of CO and NO on the defective TiO_2(110) surface, J. Phys. Chem. B **106**, 6184 (2002).

[47] D. C. Sorescu and J. T. Yates, Adsorption of CO on the TiO_2(110) surface: A theoretical study, J. Phys. Chem. B **102**, 4556 (1998).

[48] F. Rittner, B. Boddenberg, M. J. Bojan, and W. A. Steele, Adsorption of nitrogen on rutile (110): Monte Carlo computer simulations, Langmuir **15**, 1456 (1999).

[49] F. Rittner, B. Boddenberg, R. F. Fink, and V. Staemmler, Adsorption of nitrogen on rutile(110). 2. Construction of a full five-dimensional potential energy surface, Langmuir **15**, 1449 (1999).

[50] Z. W. Wang and D. J. Shu, Intrinsic interaction between in-plane ferroelectric polarization and surface adsorption, Phys. Chem. Chem. Phys. **21**, 18680 (2019).

[51] D. Li, M. H. Zhao, J. Garra, A. M. Kolpak, A. M. Rappe, D. A. Bonnell, and J. M. Vohs, Direct in situ determination of the polarization dependence of physisorption on ferroelectric surfaces, Nat. Mater. **7**, 473 (2008).

[52] J. L. Wang, B. Vilquin, and N. Barrett, Screening of ferroelectric domains on $BaTiO_3$(001) surface by ultraviolet photo-induced charge and dissociative water adsorption, Appl. Phys. Lett. **101**, 092902 (2012).

[53] R. Shao, M. P. Nikiforov, and D. A. Bonnell, Photoinduced charge dynamics on $BaTiO_3$(001) surface characterized by scanning probe microscopy, Appl. Phys. Lett. **89**, 112904 (2006).

[54] E. Maggio, N. Martsinovich, and A. Troisi, Continuum and atomistic description of excess electrons in TiO_2, J. Phys.: Condens. Matter **28**, 074004 (2016).

[55] M. Setvin, C. Franchini, X. Hao, M. Schmid, A. Janotti, M. Kaltak, C. G. Van de Walle, G. Kresse, and U. Diebold, Direct view at excess electrons in TiO_2 rutile and anatase, Phys. Rev. Lett. **113**, 086402 (2014).

[56] C. Ma, K.-J. Jin, C. Ge, and G.-Z. Yang, Strain-engineering stabilization of $BaTiO_3$-based polar metals, Phys. Rev. B **97**, 115103 (2018).

[57] D. Hickox-Young, D. Puggioni, and J. M. Rondinelli, Persistent polar distortions from covalent interactions in doped $BaTiO_3$, Phys. Rev. B **102**, 014108 (2020).

[58] B. J. Morgan and G. W. Watson, A DFT+U description of oxygen vacancies at the TiO_2 rutile (110) surface, Surf. Sci. **601**, 5034 (2007).

[59] M. Tas, E. Şaşıoğlu, S. Blügel, I. Mertig, and I. Galanakis, *Ab initio* calculation of the Hubbard U and Hund exchange J in local moment magnets: The case of Mn-based full Heusler compounds, Phys. Rev. Mater. **6**, 114401 (2022).

[60] M. García-Mota, A. Vojvodić, F. Abild-Pedersen, and J. K. Nørskov, Electronic origin of the surface reactivity of transition-metal-doped TiO_2(110), J. Phys. Chem. C **117**, 460 (2013).

[61] B. J. Morgan and P. A. Madden, Lithium intercalation into TiO_2(B): A comparison of LDA, GGA, and GGA+U density functional calculations, Phys. Rev. B **86**, 035147 (2012).

[62] A. R. Fernández, A. Schvval, M. Jiménez, G. Cabeza, and C. Morgade, Comparative study of the effect of the Hubbard coefficient U on the properties of TiO_2 and ZnO, Mater. Today Commun. **27**, 102368 (2021).

[63] R. Resta, Theory of the electric polarization in crystals, Ferroelectrics **136**, 51 (1992).

[64] D. Vanderbilt and R. D. King-Smith, Electric polarization as a bulk quantity and its relation to surface charge, Phys. Rev. B **48**, 4442 (1993).

[65] R. D. King-Smith and D. Vanderbilt, Theory of polarization of crystalline solids, Phys. Rev. B **47**, 1651 (1993).

[66] Y. Zhang, J. Sun, J. P. Perdew, and X. Wu, Comparative first-principles studies of prototypical ferroelectric materials by LDA, GGA, and SCAN meta-GGA, Phys. Rev. B **96**, 035143 (2017).

[67] T.-R. Chang, H.-T. Jeng, C.-Y. Ren, and C.-S. Hsue, Charge-orbital ordering and ferroelectric polarization in multiferroic $TbMn_2O_5$ from first principles, Phys. Rev. B **84**, 024421 (2011).

[68] G. Giovannetti and J. van den Brink, Electronic correlations decimate the ferroelectric polarization of multiferroic $HoMn_2O_5$, Phys. Rev. Lett. **100**, 227603 (2008).

[69] U. Öpik and M. H. L. Pryce, Studies of the Jahn-Teller effect. I. A survey of the static problem, Proc. R. Soc. London, Ser. A **238**, 425 (1957).

[70] I. B. Bersuker, Pseudo-Jahn-Teller effect–A two-state paradigm in formation, deformation, and transformation of molecular systems and solids, Chem. Rev. **113**, 1351 (2013).

[71] I. B. Bersuker and B. G. Vekhter, The vibronic theory of ferroelectricity, Ferroelectrics **19**, 137 (1978).

[72] I. B. Bersuker, Electronic control of molecular shapes and transformations via vibronic coupling, in *Electronic Structure and Properties of Transition Metal Compounds* (Wiley, Hoboken, 2010), Chap. 7, pp. 324–391.

[73] W. A. Al-Saidi and A. M. Rappe, Density functional study of $PbTiO_3$ nanocapacitors with Pt and Au electrodes, Phys. Rev. B **82**, 155304 (2010).